AGU PUBLICATIONS

Geophysical Research Letters

RESEARCH LETTER
10.1002/2015GL064500

Key Points:
- Fractures are observed on the surface of a comet for the first time
- Different fracture settings and topologies suggest various formation mechanisms
- Fractures may be a key driver in the evolution of the surface

Supporting Information:
- Figure S1
- Figure S2
- Texts S1 and S2 and Figure S1 and S2

Correspondence to:
M. R. El-Maarry,
mohamed.elmaarry@space.unibe.ch

Citation:
El-Maarry, M. R., et al. (2015), Fractures on comet 67P/Churyumov-Gerasimenko observed by Rosetta/OSIRIS, *Geophys. Res. Lett.*, *42*, 5170–5178, doi:10.1002/2015GL064500.

Received 11 MAY 2015
Accepted 19 JUN 2015
Accepted article online 26 JUN 2015
Published online 15 JUL 2015
Corrected 5 OCT 2015

This article was corrected on 5 OCT 2015. See the end of the full text for details.

Fractures on comet 67P/Churyumov-Gerasimenko observed by Rosetta/OSIRIS

M. R. El-Maarry[1], N. Thomas[1], A. Gracia-Berná[1], R. Marschall[1], A.-T. Auger[2], O. Groussin[2], S. Mottola[3], M. Pajola[4], M. Massironi[4,5], S. Marchi[6], S. Höfner[7], F. Preusker[3], F. Scholten[3], L. Jorda[2], E. Kührt[3], H. U. Keller[3,8], H. Sierks[7], M. F. A'Hearn[9], C. Barbieri[10], M. A. Barucci[11], J.-L. Bertaux[12], I. Bertini[4], G. Cremonese[13], V. Da Deppo[14], B. Davidsson[15], S. Debei[16], M. De Cecco[17], J. Deller[7], C. Güttler[7], S. Fornasier[11], M. Fulle[18], P. J. Gutierrez[19], M. Hofmann[7], S. F. Hviid[3], W.-H. Ip[20], J. Knollenberg[3], D. Koschny[21], G. Kovacs[7], J.-R. Kramm[7], M. Küppers[22], P. L. Lamy[2], L. M. Lara[19], M. Lazzarin[10], J. J. Lopez Moreno[19], F. Marzari[10], H. Michalik[23], G. Naletto[4,14,24], N. Oklay[7], A. Pommerol[1], H. Rickman[15,25], R. Rodrigo[26,27], C. Tubiana[7], and J.-B. Vincent[7]

[1]Physikalisches Institut, University of Bern, Bern, Switzerland, [2]Aix Marseille Université, CNRS, Laboratoire d'Astrophysique de Marseille, Marseille, France, [3]Deutsches Zentrum für Luft-und Raumfahrt, Institut für Planetenforschung, Berlin, Germany, [4]Centro di Ateneo di Studi ed Attività Spaziali, "Giuseppe Colombo", University of Padova, Padova, Italy, [5]Dipartimento di Geoscienze, University of Padova, Padova, Italy, [6]Solar System Exploration Research, Virtual Institute, Southwest Research Institute, Boulder, Colorado, USA, [7]Max-Planck-Institut für Sonnensystemforschung, Göttingen, Germany, [8]Institut für Geophysik und extraterrestrische Physik, Technische Universität Braunschweig, Braunschweig, Germany, [9]Department of Astronomy, University of Maryland, College Park, Maryland, USA, [10]Department of Physics and Astronomy, University of Padova, Padova, Italy, [11]LESIA, Observatoire de Paris, CNRS, Université Pierre et Marie Curie, Universtiy of Paris VII–Denis Diderot, Meudon, France, [12]LATMOS, CNRS/UVSQ/IPSL, Guyancourt, France, [13]INAF-Osservatorio Astronomico, Padova, Italy, [14]CNR-IFN UOS Padova LUXOR, Padova, Italy, [15]Department of Physics and Astronomy, Uppsala University, Uppsala, Sweden, [16]Department of Industrial Engineering, University of Padova, Padova, Italy, [17]Department of Industrial Engineering, University of Trento, Trento, Italy, [18]INAF-Osservatorio Astronomico di Trieste, Trieste, Italy, [19]Instituto de Astrofísica de Andalucía (CSIC), Granada, Spain, [20]Graduate Institute of Astronomy, National Central University, Chung-Li, Taiwan, [21]Scientific Support Office, European Space Agency, Noordwijk, Netherlands, [22]Operations Department, European Space Astronomy Centre/ESA, Villanueva de la Cañada, Spain, [23]Institut für Datentechnik und Kommunikationsnetze der TU Braunschweig, Braunschweig, Germany, [24]Department of Information Engineering, University of Padova, Padova, Italy, [25]PAS Space Research Center, Warszawa, Poland, [26]International Space Science Institute, Bern, Switzerland, [27]Centro de Astrobiología, CSIC-INTA, Torrejón de Ardoz, Spain

Abstract The Optical, Spectroscopic, and Infrared Remote Imaging System (OSIRIS) experiment onboard the Rosetta spacecraft currently orbiting comet 67P/Churyumov-Gerasimenko has yielded unprecedented views of a comet's nucleus. We present here the first ever observations of meter-scale fractures on the surface of a comet. Some of these fractures form polygonal networks. We present an initial assessment of their morphology, topology, and regional distribution. Fractures are ubiquitous on the surface of the comet's nucleus. Furthermore, they occur in various settings and show different topologies suggesting numerous formation mechanisms, which include thermal insulation weathering, orbital-induced stresses, and possibly seasonal thermal contraction. However, we conclude that thermal insolation weathering is responsible for creating most of the observed fractures based on their morphology and setting in addition to thermal models that indicate diurnal temperature ranges exceeding 200 K and thermal gradients of ~15 K/min at perihelion are possible. Finally, we suggest that fractures could be a facilitator in surface evolution and long-term erosion.

1. Introduction

The Rosetta spacecraft was inserted into orbit around comet 67P/Churyumov-Gerasimenko (hereinafter referred to as comet 67P) on 6 August 2014. Since then, the comet's nucleus has been extensively imaged and monitored by the Optical, Spectroscopic, and Infrared Remote Imaging System (OSIRIS) [*Keller et al.*, 2007] at high spatial resolutions reaching ~0.15 m/pixel. The OSIRIS images have shown the surface of comet 67P to be morphologically complex with several terrain types and numerous intricate features [*Sierks et al.*, 2015; *Thomas et al.*, 2015a], which include active pits [*Vincent et al.*, 2015], aeolian-like features [*Thomas et al.*, 2015b], boulder fields as well as bright, potentially water ice-rich boulders, and conical structures possibly suggestive of fluidized surface flows [*Thomas et al.*, 2015a]. In addition to these features, images of submeter resolution, acquired when the spacecraft was orbiting <20 km above the

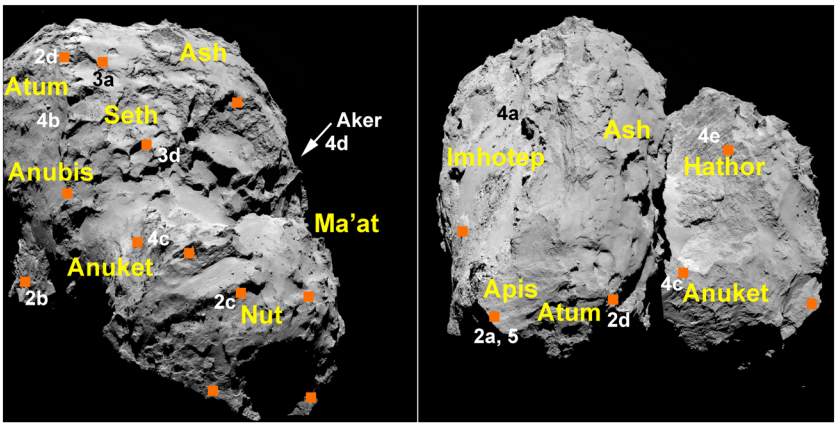

Figure 1. OSIRIS narrow-angle camera (NAC) images showing the comet in two viewing angles acquired in August 2014. Orange squares show the approximate location of some of the notable fractures observed on the surface. Labels refer to the names of some of the regions that have been defined on the surface and mentioned in this study as well as the approximate location of the other figures in the paper. The white arrow shows the approximate location of the Aker region beyond the limb. Refer to *Thomas et al*. [2015a] for more information regarding the regions and their boundaries. Image IDs: (left) NAC_2014-08-06T02.43.16.574Z_ID30_1397549100_F22 and (right) NAC_2014-08-16T13.59.14.564Z_ID30_1397549600_F22.

surface, have shown that many regions on the comet, especially those composed of consolidated materials [*Thomas et al*., 2015a; *El-Maarry et al*., 2015], are fractured forming various patterns. We present these fractures here in detail for the first time and give an initial assessment of their morphology, topology, and distribution.

2. Methods and Data Sets

OSIRIS consists of a narrow-angle (38.4 × 38.7 mrad field of view (FOV)) camera (NAC) designed for the mapping of the comet's surface with 12 filters covering the spectral range of 250–1000 nm in high spatial resolution, and a wide-angle (198 × 211 mrad FOV) camera, which is optimized for gas and dust studies in the vicinity of the comet with 14 filters in the spectral range of 240–720 nm [*Keller et al*., 2007]. In this study, we concentrate on NAC images acquired from the time of first orbit insertion (6 August 2014) to 1 March 2015, in particular those taken with the "orange" filter (centered at ~647 nm) during close orbits (~8–18 km above the surface of the nucleus) because high spatial resolution is required to identify and characterize most of the fractures. Due to the need for an accurate knowledge of the size scale of the features of interest, we employed a technique by which the information from the most recent shape models were combined with 3-D visualization tools to extract the exact spatial resolution of the OSIRIS images at the features of interest (refer to supporting information Text S1 for details).

3. Observations

Comet 67P has a bilobed shape (Figure 1) comprising a large lobe (4.1 × 3.3 × 1.8 km, called the body) connected to a smaller lobe (2.6 × 2.3 × 1.8 km, called the head) by a short "neck region" [*Sierks et al*., 2015]. A regional assessment of the surface morphology has resulted in the classification of the comet's surface into distinctive regions based on morphological and structural attributes [*Thomas et al*., 2015a; *El-Maarry et al*., 2015, Figure 1]. Our initial assessment of the fractures distribution suggests that they are globally present on the surface of the nucleus (Figure 1), particularly in consolidated regions [*Thomas et al*., 2015a], wherever images with high enough spatial resolution are available. These fractures are present in one of four distinctive settings briefly described below.

3.1. Fracture Networks

This is the most common setting observed generally on quasi-flat surfaces (Figure 2). The fractures are generally narrow (submeter in width) and resemble mode-I tensile fractures [e.g., *Gudmundsson*, 2011]. The fractures create irregular polygonal patterns in many cases. Fractures vary greatly in length from a few

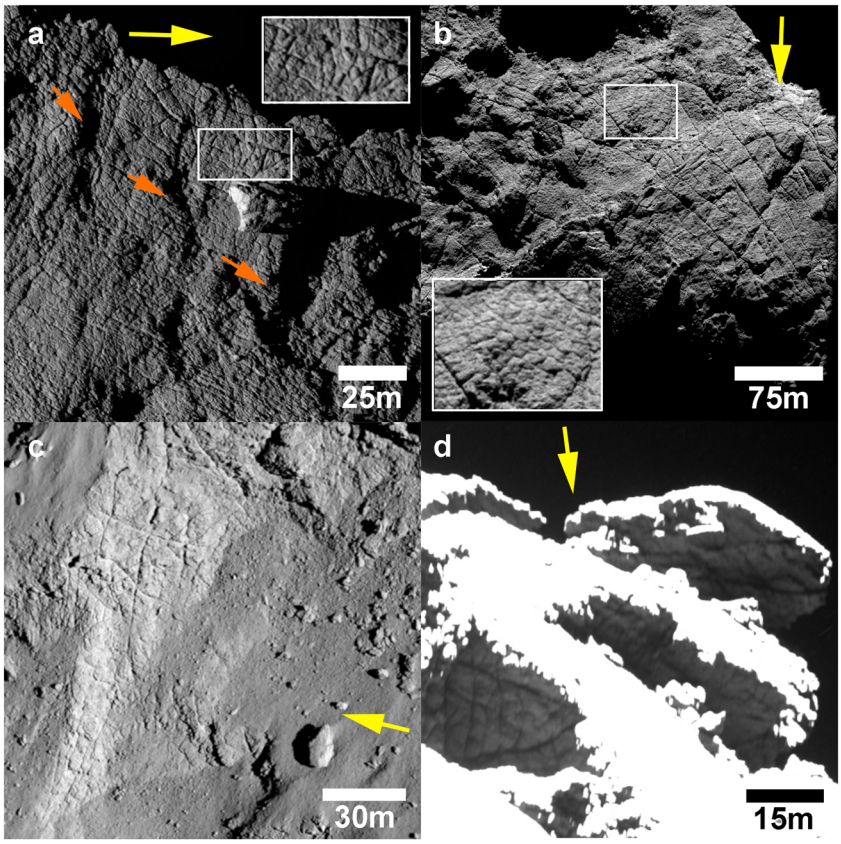

Figure 2. Fracture networks on the surface of the comet. Yellow arrows show the approximate direction of sunlight. (a) Polygonal fractures on the edge of the Apis region on the body lobe (Figure 1). Upon close inspection (inbox), the patterns are composed of irregular 2–5 m wide polygons. Also to note is the pattern of shadows running from the top left to the lower right (orange arrows), which may indicate vertical displacement. (b) A pervasively fractured region at the edge of the Atum regions close to the neck. Fractures vary greatly in length and mode of intersection forming highly irregular polygons. The longest visible facture is ~250 m. Within this irregular pattern, a more regular pattern of 2–6 m wide polygons is visible in a number of regions (inbox). (c) Regular patterns in at the edge of Nut depression creating ~15 m wide polygons with orthogonal fracture intersections. (d) Polygonal patterns on the edge the ridge separating Anubis/Atum from Ash and Seth regions. Image has been overexposed to highlight the shadowed features. Smaller embedded polygons are 2–5 m wide. Image IDs: (Figure 2a) NAC_2015-02-14T10.35.40.393Z_ID00_1397549000_F82, (Figure 2b) NAC_2014-09-30T08.54.41.560Z_ID30_1397549700_F22, (Figure 2c) NAC_2014-11-12T15.18.52.608Z_ID30_1397549600_F22, and (Figure 2d) NAC_2014-10-14T18.58.11.922Z_ID30_1397549400_F22.

meters to ~250 m in length. Similarly, the angles of intersections of the fractures are variable. However, some locations (e.g., Figure 2c) show orthogonal intersections that may be indicative of a slowly evolving uniformly stressed system [*El-Maarry et al*., 2012, 2014, and references therein]. Interestingly, a number of locations (e.g., Figures 2a and 2b) display embedded hummocky morphology that could indicate the presence of smaller and more ordered polygonal fractures morphologically similar to periglacial high-centered thermal contraction polygons on Earth and Mars [e.g., *Marchant et al*., 2002; *Levy et al*., 2010].

3.2. Fractures on Cliffs

Fractures are similarly observed on the edges of cliffs (Figure 3) in a number of regions but are mostly observed in the Seth region in the weakly consolidated units, which were referred to as "brittle" units by *Thomas et al*. [2015a]. In some locations, the feet of the fractured cliffs are covered by debris deposits, which suggest continuous mass wasting events triggered by the fracturing process. Other locations show what appear to be recently formed fractures crosscutting older ones (Figures 3b and 3c), which suggests a periodically continuous process. Incidentally, the Philae lander sent images prior to its hibernation showing a heavily fractured overhang (informally dubbed "Perihelion cliff," http://www.esa.int/spaceinimages/Images/2015/01/Perihelion_Cliff),

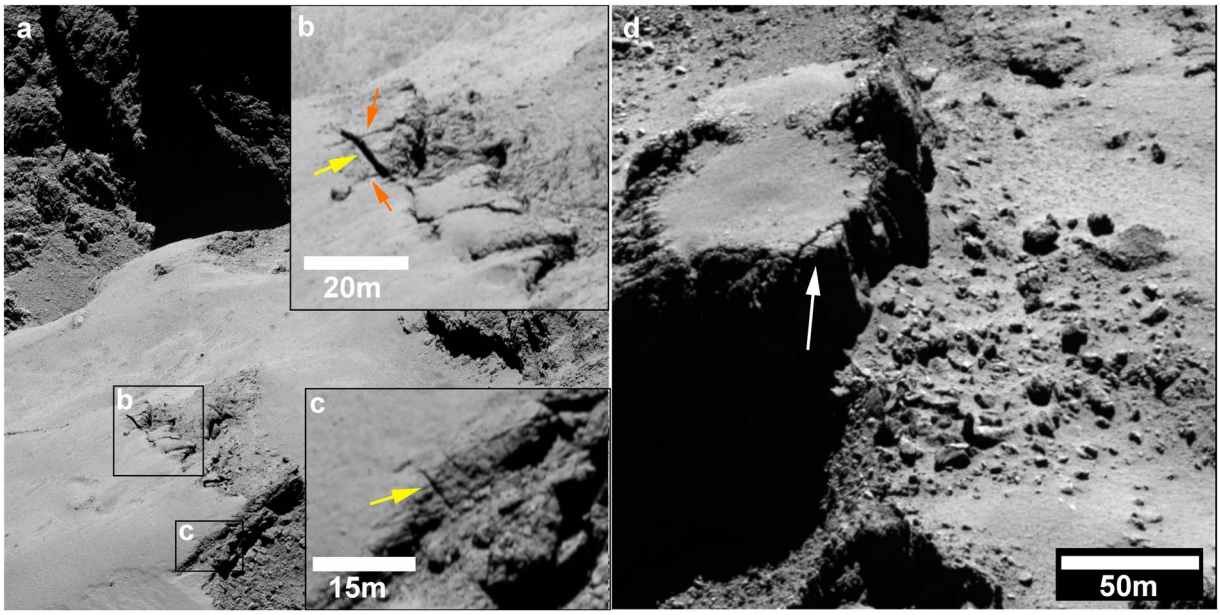

Figure 3. (a) NAC image of the Ash region in the foreground and the regions of Hathor and Anuket in the background. Boxes show the locations of the highlighted regions in Figures 3b and 3c. (b) Close-up of the fractured scarp showing what appears to be a new fracture (yellow arrow) cross cutting two older fractures (orange arrows). The new fracture is 100–125 cm wide and is expected to lead to mass wasting of the fractured scarp. (c) Another small fracture (yellow arrow) that appears to cut though the scarp edge and the smooth coating on the top, which is a morphologic characteristic of the Ash region. (d) Cropped NAC image of another mesa in the Seth region showing a similarly fractured scarp (arrowed) and a debris field in at the foot of the cliff suggesting a progressive process of mass wasting. Image ID: (Figures 3a–3c) NAC_2015-02-14T10.18.40.360Z_ID00_1397549000_F82. (Figures 3d) NAC_2014-10-01T23.29.53.545Z_ID30_1397549300_F22.

which may indicate that this fracture setting is common on the surface of the comet in addition to polygonally patterned systems (section 3.1).

3.3. Fractured Boulders

Irregular fractures are observed on a number of large (20–60 m wide) boulders scattered on the surface of the comet (Figure 4). In some cases, the fractures appear to have pervasively fragmented the boulders (Figure 4a), whereas in other cases, they appear to be confined to sharp and polished surfaces (Figure 4b), which may represent an erosional sequence where boulders become increasingly fragmented with time. Fractures are mostly linear but in some instances may form conchoidal patterns (Figure 4b).

3.4. Unique/Special Fracture Systems

Apart from the three main settings described above, three unique features are observed on the surface: (1) a ~500 m long fracture system in the Anuket region (Figure 4c), (2) a 200 m long angular fracture system in the Aker region (Figure 4d), and (3) a set of parallel longitudinal fractures on the cliff of Hathor (Figure 4e). These unique features have already been mentioned briefly in recent publications [e.g., *Thomas et al.*, 2015a; *Marchi et al.*, 2015].

In the case of the Anuket feature, the morphology of the fracture and the lack of visible shear displacement suggest that it could be either tensile or compressive in nature. However, no associated ridges or thrust faults indicative of a compressive regime are observed in the near vicinity. In addition, closer inspection of this fracture reveals that it is in fact composed of a number of similarly aligned smaller fractures (Figure 4c), which suggests that a prolonged tensile stress field affects this region. Similarly, the angular fracture system in Aker is an isolated feature in the context of the surrounding morphology. Moreover, it is the only feature that shows possible signs of out-of-plane shear displacement (mode III) in addition to mode I, which is suggestive of a highly complex yet localized stress field.

Finally, the Hathor cliff displays an extended set of fractures which cut almost perpendicularly a set of multiple strata ~900 m wide (see Figure S1). Some of the fractures (~200 of them) are $>$ 350 m in length. However, more than 90% of them are smaller than 150 m long.

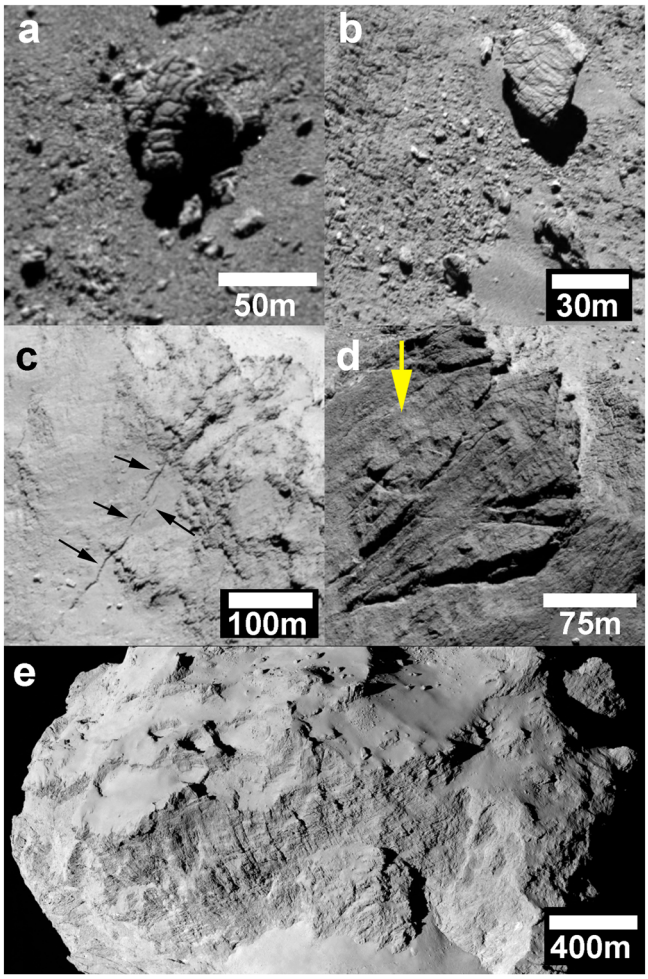

Figure 4. (a, b) NAC images showing fractured boulders in the Imhotep (Figure 4a) and Atum (Figure 4b) regions. Fracturing in the Imhotep boulder is so pervasive it has led to fragmentation of the 60 m wide boulder. (c) 500 m long fracture system in the Anuket region. The linear feature consists in fact of a number of aligned smaller fractures (black arrows). (d) Angular fracture system in the Aker region. Yellow arrow shows the direction of sunlight. (e) Longitudinal-parallel fracture system on the Hathor cliff. Image IDs: (Figure 4a) NAC_2014-09-29T12.59.59.587Z_ID30_1397549100_F22, (Figure 4b) NAC_2015-02-14T09.30.51.350Z_ID00_1397549000_F82, (Figure 4c) NAC_2014-08-26T06.42.56.564Z_ID30_1397549200_F22, (Figure 4d) NAC_2014-09-19T09.38.55.332Z_ID30_1397549100_F22, and (Figure 4e) NAC_2014-08-07T20.37.34.564Z_ID30_1397549300_F22.

4. Potential Formation Mechanisms

With the exception of one notable feature (the Aker fracture system), there is little evidence for the presence of shear-dominated fractures. Similarly, no tectonic thrust structures are observed in the vicinity of the observed fractures making the role of compressional stresses unclear at best. Therefore, we conclude that most of the fractures we observe in this study are driven by tensile stresses.

On Earth and other planetary bodies such as Mars, tensile fractures develop through three common processes: (1) loss of volatile materials (e.g., desiccation), (2) thermal contraction or contraction/expansion cycles, and (3) tectonic processes.

Comets as well as other small bodies devoid of a permanent thick atmosphere are known to undergo high fluctuations in surface temperatures on diurnal and seasonal scales, as well as subsurface temperatures depending on the thermal conductivity of the surface materials. Our first-order thermal models following the algorithm of *Spencer et al.* [1989] for comet 67P result in diurnal surface temperature fluctuations of ~120 K–350 K in illuminated regions at perihelion (1.3 AU, Figure 5). Assuming a thermal inertia of 50 $J\,K^{-1}\,m^{-2}\,s^{-0.5}$ consistent with measurements by the Microwave Instrument on the Rosetta Orbiter (MIRO) [*Gulkis et al.*, 2015], and measurements at other comets [e.g., *Groussin et al.*, 2013], we derive high temperature gradients exceeding 15 K/min for short periods (Figure 5).

The large temperature variations in terms of estimated gradients and diurnal range may lead to fracturing either on the short term as thermal shock or on the long term as thermal fatigue, respectively, in a process collectively referred to as thermal insolation weathering [*Hall and Thorn*, 2014, and references therein] (refer to supporting information Text S2 for additional information). This process is a common weathering process on Earth and is expected to fracture materials even at stress levels significantly lower than their bulk tensile strength through the development of microcracks that act to weaken the affected material.

Thermal weathering has been invoked to explain mechanical breakdown (including fractured boulders) in arid landscapes on Earth [e.g., *McFadden et al.*, 2005], Mars [e.g., *Viles et al.*, 2010; *Eppes et al.*, 2015], and asteroids [e.g., *Dombard et al.*, 2010]. In addition, thermal stresses have been invoked recently to explain the production of debris on airless bodies [*Molaro et al.*, 2015], including asteroids [*Delbo et al.*, 2014] as well as the formation of lineations on asteroids [*Dombard and Freed*, 2002].

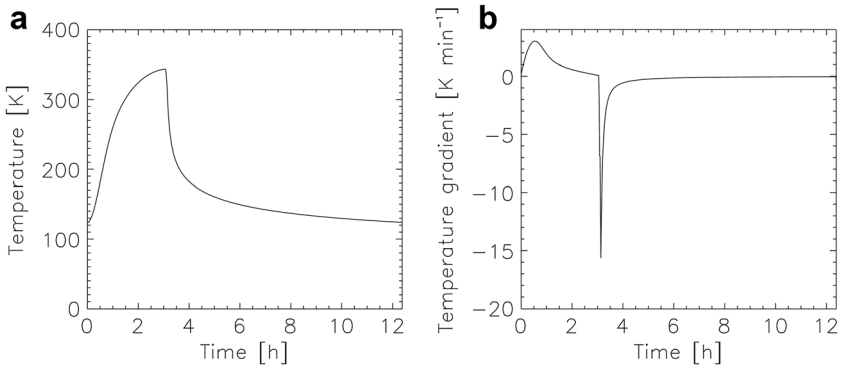

Figure 5. (a) Surface temperature profile and (b) a theoretical calculation for a maximum temporal thermal gradient that might be expected at 67P in its current orbit. The model assumes an insolation profile going from dawn (0 h) to midday at which point the Sun is at zenith. At exactly this time, the surface passes into shadow over a period of 2 min (simulating the approximate diameter of the Sun). The surface cools rapidly for the rest of the 12.4 h rotation period. A thermal inertia of 50 J K^{-1} m^{-2} $s^{-0.5}$ has been assumed for the surface consistent with measurements by MIRO [*Gulkis et al*., 2015] and measurements at other comets [e.g., *Groussin et al*., 2013]. Solution of the 1-D thermal balance equation when the comet is at perihelion (1.3 AU) shows that the diurnal temperature range exceeds 200 K. In addition, d*T*/d*t* can exceed −15 K min^{-1} under these conditions. The heating during the morning reaches a peak of about +3 K min^{-1}. It should be noted that *Delbo et al*. [2014] have demonstrated that thermal weathering maybe a key factor in debris production on asteroids through fracturing using temperature gradients that are almost a factor of 5 less than what we derive as an upper limit for comet 67P.

With regards to diurnal temperature ranges, our derived range of ~230 K is also higher than that modeled by *Delbo et al*. [2014] (190 K), and comparable to estimated diurnal ranges for the Moon (~250–300 K) [*Vasavada et al*., 1999], which have been shown by *Molaro et al*. [2015] to induce thermomechanical weathering of the Lunar surface through thermal fatigue.

It should also be noted that since the temperature of the comet is expected to be very low even at depth throughout its revolution around the Sun, irrespective of the large diurnal changes, fractures are expected to develop readily because of the brittle nature of the surface materials and are even expected to propagate to depths of up to 25 times that of the diurnal thermal skin depth (estimated to be ~6 mm by MIRO, [*Gulkis et al*., 2015]) assuming an ice-rich silicate substrate [*Maloof et al*., 2002].

Moreover, given high enough thermal inertia (and the presence of subsurface ice), seasonal thermal skin depths may penetrate to significant depths to affect subsurface temperatures and potentially lead to the development of cracks as a result of seasonal thermal contraction. The possible presence of embedded small polygons resembling high-centered seasonal thermal contraction polygons within larger irregular fractures systems (section 3.1) poses interesting questions because polygons tend to become more geometrically ordered as they become larger and commonly vary with size from smaller hexagonal irregular polygons to larger more ordered four-sided polygons with orthogonal or near-orthogonal fracture intersections [e.g., *El-Maarry et al*., 2010, and references therein]. Generally speaking, larger polygons correspond to deeper fractures, which in turn correspond to thicker stressed zones that take significantly longer time to develop [e.g., *Lachenbruch*, 1961, *El-Maarry et al*., 2012]. However, if these small embedded features are indeed polygonal fracture systems, then what is observed on comet 67P is contrary to the conventional geometrical evolution of tensile stress-induced fracture systems, which may indicate two different formation mechanisms for the irregular patterns and the embedded, ordered ones.

4.1. Other Formation Mechanisms

The presence of fractures in various settings in addition to the presence of unique features such as the Aker, Anuket, and Hathor fracture systems indicates that further mechanisms may be at work including tectonic processes that are possibly orbit induced. For example, the length of the Anuket fracture system and the fact that it does not display any additional parallel or intersecting sets of fractures in its vicinity argues against common tensile processes that tend to create a widespread stress field-generating networks of cracks. Moreover, the location of the feature within the neck region between the comet's two major lobes

Table 1. A Summary of Possible Formation Mechanisms and Proposed Methods of Testing and Validation for Various Fractures[a]

Features	Morphology	Location	Formation Mechanism	Testing and Validation
Polygonal networks	Fractures of variable length forming irregular polygons. Some embedded hummocky features may be candidate small ordered polygons.	Flat surfaces with notable examples in the Apis, Nut, and Atum regions.	**Thermal insolation weathering**, thermal contraction, sublimation-driven desiccation?	Modeling, lab testing with possible constraints on thermophysical properties of the surface as well as the detection of near-surface ice by Philae.
Fractured cliffs	Fractures on the edges of cliffs and scarps that usually display talus deposits at its feet.	Mainly in the Seth region and exposed scarps in the dusty Ash and Ma'at regions.	**Thermal insolation weathering**, activity-induced stresses?	Monitoring of notable sites for changes (i.e., mechanical failure or development of new fractures).
Fractured boulders	Fractures on large boulders. Some boulders being heavily fragmented.	Probably global.	**Thermal insolation weathering**, mechanical fracturing due to tumbling down.	Monitoring of possibly newly formed boulders following intensive activity after perihelion passage.
		Currently Unique Features		
Anuket feature	~500 m long fracture system.	Anuket region close to the neck.	**Orbital-induced or tidal-like forces**, activity-induced torques.	Modeling, monitoring for changes during perihelion passage.
Aker feature	~200 m long angular fracture system.	Aker region.	**Orbital-induced or tidal-like forces**, activity-induced torques.	Modelling, monitoring for changes during perihelion passage.
Hathor fractures	Long parallel fractures along the Hathor cliff.	Hathor.	**Collisions**, thermal insolation weathering.	Modelling of early cometary formation scenarios.

[a]The mechanisms marked in bold are the preferred candidate mechanisms in this study.

suggests that the Anuket feature may possibly be caused by rotation- or orbit-induced stresses. In particular, jet activity and solar tidal forces result in torques that can generate forced precession of the body. Such an excited rotation state induces internal stresses, which could result in the generation of the observed cracks.

On the other hand, the presence of fractures on the cliffs of Hathor in proximity to the neck region may suggest a collisional origin following formation in the trans-Neptunian primordial disk or a result of subsequent collisional evolution within the scattered disk assuming the comet is a contact binary [*Marchi et al.*, 2015]. Table 1 summarizes our different formation hypotheses regarding the various observed fractures and ways of possibly testing or validating them by further investigations from the Rosetta mission.

5. Implications

5.1. Fractures as Erosional Triggers

As presented in section 3.2, fractures are observed on cliffs (Figure 3). Closer inspection shows that such locations tend to show talus-like deposits at the feet of escarpments, which suggests that fractures represent the first stage in driving further mass wasting and eventual failure of the cliff material in a landslide-like process. This process should act on the long term to mechanically erode the surface of the comet and flatten the landscape. The fact that the surface displays many rough terrains such as the Seth region suggests that either the comet has not gone through many erosional cycles or there are other processes that conversely act to roughen the surface topography such as episodes of explosive jet activity. Indeed, the presence of deep depressions with sharp-looking scarps on both lobes of the comet suggests that such processes maybe active on the surface [*Thomas et al.*, 2015a; *El-Maarry et al.*, 2015].

5.2. Fractures as Possible Markers of Shallow Subsurface Ice

On Earth and other planetary bodies such as Mars, the presence of thermal contraction polygons is a strong indicator of the presence of subsurface ice [e.g., *French*, 2007, and references therein]. While most of the polygonal fractures observed on the surface of 67P exhibit patterns that are highly irregular, there are some fractures that display orthogonal intersections. Furthermore, there are indications of smaller embedded polygons similar to periglacial high-centered polygons. The presence of seasonal thermal

contraction polygons would suggest the presence of (1) near-subsurface ice and, by consequence, (2) high thermal inertia regions.

Other instruments onboard the Rosetta spacecraft, namely, the Visible Infrared and Thermal Imaging Spectrometer (VIRTIS) and MIRO (section 4) have recently reported that the near surface (~top tens of millimeters) of the surface is mostly volatile free yet organic rich [*Capaccioni et al*., 2015] and has a very low thermal inertia in the range of 10–50 $J\,K^{-1}\,m^{-2}\,s^{-0.5}$ [*Gulkis et al*., 2015]. However, such measurements, while being well representative of the surface of the comet overall, do not necessarily account for minor heterogeneities or the near sub-subsurface below these instruments' spatial resolution (approximately tens to hundreds of meters) and vertical sensitivity (a few to tens of millimeters), respectively. Indeed, a close inspection at high (<0.5 m/pixel) spatial resolution shows that even in regions of the comet that do not appear to be dominated by dust coatings such as Ash and Ma'at (Figure 1) [*Thomas et al*., 2015a] there appears to be a significant amount of dust that could be contributing to the globally low thermal inertia. An example is shown in Figure S2 where a wider view of Figure 2a is showing thin coatings of dust that appear to be fading away and exposing the underlying fractured terrain.

Furthermore, numerous studies using various modeling approaches and lab experiments such as KOSI [*Kochan et al*., 1989; *Sears et al*., 1999, and references therein] to simulate the evolution of cometary nuclei conclude that sintering of ice or recondensation of sublimated water vapor following sublimation has the following consequences: (1) hardening of the near-surface ice layer [e.g., *Seiferlin et al*., 1995; *Kossacki et al*., 1997, 1999], (2) increase of thermal conductivity, especially in the presence of organics [e.g., *Kömle et al*., 1996], and (3) development of a millimeter-thick surface dust layer [e.g., *Grün et al*., 1993; *Kossacki et al*., 1997; *Pommerol et al*., 2015], which should act to lower the global surface thermal inertia and mask the thermophysical properties of the materials directly underneath thus offering a possible explanation for the VIRTIS and MIRO measurements. The combination of these factors (especially 1 and 2) would favor the development of large fractures by increasing the surface stiffness or Young's modulus [e.g., *Gudmundsson*, 2011], thereby allowing high stresses to develop before fracturing, and the depth of penetration of the thermal wave, thereby allowing the development of thick stressed regions, and consequently deeper and wider-spaced fractures [e.g., *Lachenbruch*, 1961]. However, we note that the relevance of findings from such lab experiments (particularly those of the KOSI experiments) has been challenged because of the difficulties involved in simulating cometary conditions in a lab [e.g., *Keller and Markiewicz*, 1991]. Therefore, more in-depth modeling and lab work are needed to investigate these aspects. A resumption of operations by the Philae lander may also help by possibly detecting and characterizing near-subsurface ice or more generally by constraining some of the thermophysical properties of the surface needed for accurate modeling and preparation of suitable lab analogs.

Acknowledgments

OSIRIS was built by a consortium of the Max-Planck-Institut für Sonnensystemforschung, in Göttingen, Germany; CISAS-University of Padova, Italy; the Laboratoire d'Astrophysique de Marseille, France; the Instituto de Astrofísica de Andalucia, CSIC, Granada, Spain; the Research and Scientific Support Department of the European Space Agency, Noordwijk, The Netherlands; the Instituto Nacional de Técnica Aeroespacial, Madrid, Spain; the Universidad Politćhnica de Madrid, Spain; the Department of Physics and Astronomy of Uppsala University, Sweden; and the Institut für Datentechnik und Kommunikationsnetze der Technischen Universität Braunschweig, Germany. The support of the national funding agencies of Germany (DLR), France (CNES), Italy (ASI), Spain (MEC), Sweden (SNSB), and the ESA Technical Directorate is gratefully acknowledged. We thank the ESA teams at ESAC, ESOC, and ESTEC for their work in support of the Rosetta mission. The images used in this study will be released through ESA's Planetary Science Archive (http://www.rssd.esa.int/index.php?project=PSA&page=rosetta). They are available through the first author upon request using the image IDs mentioned in the study. The authors would also like to thank Jamie Molaro and an anonymous reviewer for their critical review of the paper.

The Editor thanks Andrew Cheng and an anonymous reviewer for their assistance in evaluating this paper.

References

Capaccioni, F., et al. (2015), The organic-rich surface of comet 67P/Churyumov-Gerasimenko as seen by VIRTIS/Rosetta, *Science*, *347*, doi:10.1126/science.aaa0628.

Delbo, M., G. Libourel, J. Wilkerson, N. Murdoch, P. Michel, K. T. Ramesh, C. Ganino, C. Verati, and S. Marchi (2014), Thermal fatigue as the origin of regolith on small asteroids, *Nature*, *508*, 233–236, doi:10.1038/nature13153.

Dombard, A. J., and A. M. Freed (2002), Thermally induced lineations on the asteroid Eros: Evidence of orbit transfer, *Geophys. Res. Lett.*, *29*(16), 65-1–65-4, doi:10.1029/2002GL015181.

Dombard, A. J., O. S. Barnouin, L. M. Prockter, and P. C. Thomas (2010), Boulders and ponds on the Asteroid 433 Eros, *Icarus*, *210*, 713–721, doi:10.1016/j.icarus.2010.07.006.

El Maarry, M. R., W. J. Markiewicz, M. T. Mellon, W. Goetz, J. M. Dohm, and A. Pack (2010), Crater floor polygons: Desiccation patterns of ancient lakes on Mars?, *J. Geophys. Res.*, *115*, E10006, doi:10.1029/2010JE003609.

El-Maarry, M. R., J. Kodikara, S. Wijessoriya, W. J. Markiewicz, and N. Thomas (2012), Desiccation mechanism for formation of giant polygons on Earth and intermediate-sized polygons on Mars: Results from a pre-fracture model, *Earth Planet. Sci. Lett.*, *323*, 19–26.

El-Maarry, M. R., W. Watters, N. McKeown, J. Carter, E. Noe Dobrea, J. Bishop, A. Pommerol, and N. Thomas (2014), Putative desiccation cracks on Mars: A synthesis from modeling analogue-field studies, and global observations, *Icarus*, *241*, 248–268.

El-Maarry, M. R., et al. (2015), Regional surface morphology of comet 67P/Churyumov-Gerasimenko using the OSIRIS Camera Onboard Rosetta, 46th Lunar Planet. Sci. Congr., abstract #1829.

Eppes, M.-C., A. Willis, J. Molaro, S. Abernathy, and B. Zhou (2015), Cracks in Martian boulders exhibit preferred orientations that point to solar-induced thermal stress, *Nat. Commun.*, *6*, 6712, doi:10.1038/ncomms7712.

French, H. M. (2007), *The Periglacial Environment*, 3rd ed., pp. 458, John Wiley.

Groussin, O., et al. (2013), The temperature, thermal inertia, roughness and color of the nuclei of Comets 103P/Hartley 2 and 9P/Tempel 1, *Icarus*, *222*, 580–594.

Grün, E., et al. (1993), Development of a dust mantle on the surface of an insolated ice-dust mixture: Results from the KOSI-9 experiment, *J. Geophys. Res.*, *98*(E8), 15,091–15,104, doi:10.1029/93JE01134.

Gudmundsson, A. (2011), *Rock Fractures in Geological Processes*, pp. 592, Cambridge Univ. Press, U. K.
Gulkis, S., et al. (2015), Subsurface properties and early activity of comet 67P/Churyumov-Gerasimenko, *Science*, *347*, doi:10.1126/science.aaa0709.
Hall, K., and C. E. Thorn (2014), Thermal fatigue and thermal shock in bedrock: An attempt to unravel the geomorphic processes and products, *Geomorphology*, *206*, 1–13.
Keller, H. U., and W. J. Markiewicz (1991), KOSI?, *Geophys. Res. Lett.*, *18*, 249–252, doi:10.1029/90GL02591.
Keller, H. U., et al. (2007), OSIRIS—The scientific camera system onboard Rosetta, *Space Sci. Rev.*, *128*, 433–506.
Kochan, H., et al. (1989), Comet simulation experiments in the DFVLR space simulators, *Adv. Space Res.*, *9*(3), 113–122.
Kömle, N. I., G. Kargl, K. Thiel, and K. Seiferlin (1996), Thermal properties of cometary ices and sublimation residua including organics, *Planet. Space Sci.*, *44*, 675–689.
Kossacki, K. J., N. I. Kömle, J. Leliwa-Kopystynski, and G. Kargl (1997), Laboratory investigation of the evolution of cometary analogs: Results and interpretation, *Icarus*, *128*, 127–144.
Kossacki, K. J., S. Szutowicz, and J. Leliwa-Kopystynski (1999), Comet 46P/Wirtanen: Evolution of the subsurface layer, *Icarus*, *142*, 202–218.
Lachenbruch, A. H. (1961), Depth and spacing of tension cracks, *J. Geophys. Res.*, *66*(12), 4273–4292, doi:10.1029/JZ066i012p04273.
Levy, J. S., D. R. Marchant, and J. W. Head (2010), Thermal contraction crack polygons on Mars: A synthesis from HiRISE, Phoenix, and terrestrial analog studies, *Icarus*, *206*(1), 229–252, doi:10.1016/j.icarus.2009.09.005.
Maloof, A. C., J. B. Kellogg, and A. M. Anders (2002), Neoproterozoic sand wedges: Crack formation in frozen soils under diurnal forcing during a snowball Earth, *Earth Planet. Sci. Lett.*, *204*(1–2), 1–15, doi:10.1016/S0012-821X(02)00960-3.
Marchant, D. R., A. R. Lewis, W. M. Phillips, E. J. Moore, R. A. Souchez, G. H. Denton, D. E. Sugden, N. Potter Jr., and G. P. Landis (2002), Formation of patterned ground and sublimation till over Miocene glacier ice in Beacon Valley, southern Victoria Land, Antarctica, *Geol. Soc. Am. Bull.*, *114*, 718–730.
Marchi, S., et al. (2015), The geomorphology of comet 67P: Implications for the past collisional evolution and formation, 46th Lunar Planet. Sci. Conf., abstract #1532.
McFadden, L. D., M.-C. Eppes, A. R. Gillespie, and B. Hallet (2005), Physical weathering in arid landscapes due to diurnal variation in the direction of solar heating, *GSA Bull.*, *117*, 161–173, doi:10.1130/B25508.1.
Molaro, J. L., S. Byrne, and S. A. Langer (2015), Grain-scale thermoelastic stresses and spatiotemporal temperature gradients on airless bodies, implications for rock breakdown, *J. Geophys. Res. Planets*, *120*, 255–277, doi:10.1002/2014JE004729.
Pommerol, A., B. Jost, O. Poch, M. R. El-Maarry, B. Vuitel, and N. Thomas (2015), Laboratory characterization of the sublimation of icy planetary analogues: First results of the SCITEAS experiment, *Planet. Space Sc.*, *109–110*, 106–122.
Sears, D. W. G., H. W. Kochan, and W. F. Huebner (1999), Laboratory simulation of the physical processes occurring on and near the surfaces of comet nuclei, *Meteorit. Planet. Sci.*, *34*, 497–525.
Seiferlin, K., T. Spohn, and J. Benkhoff (1995), Cometary ice texture and the thermal evolution of comets, *Adv. Space Res.*, *15*, 35–38.
Sierks, H., et al. (2015), On the nucleus structure and activity of comet 67P/Churyumov-Gerasimenko, *Science*, *347*, doi:10.1126/science.aaa1044.
Spencer, J. R., L. A. Lebofsky, and M. V. Sykes (1989), Systematic biases in radiometric diameter determinations, *Icarus*, *78*, 337–354.
Thomas, N., et al. (2015a), The morphological diversity of comet 67P/Churyumov-Gerasimenko, *Science*, *347*, doi:10.1126/science.aaa0440.
Thomas, N., et al. (2015b), Evidence and modelling of dust transport on the nucleus of comet 67P/Churyumov-Gerasimenko, 46th Lunar Planet. Sci. Conf., abstract #1712.
Vasavada, A. R., D. A. Paige, and S. E. Wood (1999), Near-surface temperatures on Mercury and the Moon and the stability of polar ice deposits, *Icarus*, *141*, 179–193, doi:10.1006/icar.1999.6175.
Viles, H., B. Ehlmann, C. F. Wilson, T. Cebula, M. Page, and M. Bourke (2010), Simulating weathering of basalt on Mars and Earth by thermal cycling, *Geophys. Res. Lett.*, *37*, L18201, doi:10.1029/2010GL043522.
Vincent, J.-B., et al. (2015), A glimpse into the underworld: Active pits on comet 67P, 46th Lunar Planet. Sci. Conf., abstract #2041.

Erratum

In the originally published version of this article,an error appeared in the legend of Figure 3d. The following has since been corrected, and this version may be considered the authoritative version of record. In the legend of Figure 3d, “Ash region” has been corrected to “Seth region”.